RSC Advances

PAPER

View Article Online
View Journal | View Issue

Cite this: *RSC Adv.*, 2019, **9**, 17016

Hydrothermal-assisted shearing exfoliation for few-layered MoS_2 nanosheets

Pei-Rong Wu, Zan Liu and Zhi-Lin Cheng *

Received 19th March 2019
Accepted 17th May 2019

DOI: 10.1039/c9ra02102g

rsc.li/rsc-advances

The exfoliation of bulk MoS_2 into few layers has attracted considerable attention as 2D nanomaterials in the past decade. We developed a facile approach for producing MoS_2 nanosheets by hydrothermal-assisted shearing exfoliation based on organic-free strategy. This original exfoliation was highly efficient for large-scale production and sustainable for the environment. The thickness of the as-exfoliated MoS_2 nanosheets was about 4–6 layers, and the lateral size became smaller from hydrothermal processing to shearing. The hydrothermal processing with the participation of ammonium carbonate played an important role in hydrothermal-assisted shearing exfoliation. As a prospective application, the antifriction performance of the as-exfoliated MoS_2 nanosheets in oil was evaluated using a ball-on-ball mode. Evidently, the average friction coefficient and wear scar diameter of 0.08 wt% MoS_2-based oil dropped to about 20.66% and 47.27% relative to those of the base oil, which exhibited an excellent antifriction and antiwear ability.

1. Introduction

MoS_2 nanosheets, as inorganic analogues of graphene, have excellent properties that are useful in many practical applications as catalysts,[1,2] in batteries,[3,4] sensors,[5] nanotransistors,[6] hydrogen storage devices,[7] supercapacitors,[8] and lubricants,[9,10] due to the band gap of 1.2–1.8 eV and the layered structure with S–Mo–S monolayers interacted *via* van der Waals forces. At present, the bulk MoS_2 has been widely used as an anti-wear additive in solid greases,[11] but it cannot be used in liquid lubricants due to its unstable dispersion. The specific surface area of the bulk MoS_2 was increased through nanotechnology to obtain MoS_2 nanosheets and enhanced the stable dispersion in liquid lubricants. Rajendhran *et al.*[12] exfoliated the bulk MoS_2 to Ni–MoS_2 nanosheets by ultrasonication and reflux techniques. The friction results revealed that the average friction coefficient (COF) and average wear scar diameter (AWSD) of 0.5 wt% Ni–MoS_2-based oil decreased by 40–50% and 15–20% compared to those of the base oil due to its small size and surface modification behavior. To date, many top-down designs for preparing monolayer or multilayer MoS_2 nanosheets have been successfully achieved, such as micromechanical peeling,[13] electrochemical exfoliation,[14] liquid-phase ultrasound,[15] ion intercalation[16] and shearing method.[17] In contrast to bottom-up methods with high cost and serious pollution,[18–20] the exfoliation method for MoS_2 nanosheets was more conducive to exert its application in oil as additive due to the lateral size being of less influence on the friction of the oil. The liquid-phase exfoliation assisted with physical means such as ultrasonication and shearing is of preferable advantage for high quality and scalable output.[21–23] In particular, a kitchen blender was used to exfoliate bulk MoS_2 into nanosheets with a mean thickness of 4.6 nm (ref. 24) and the number of MoS_2 nanosheet layers is mostly less than four layers.[25] However, these liquid-phase exfoliations for nanosheets based on organic solvents were expensive and time consuming because the removal of the toxic and high boiling organic solvents after an exfoliating process accounted for an unprecedented challenge for large scale productions.[26] Hence, it is urgent to develop a highly efficient method for exfoliating MoS_2 nanosheets.

In this study, we adopted a facile exfoliation method based on hydrothermal-shearing exfoliation to access MoS_2 nanosheets. The structure and change of the exfoliated MoS_2 nanosheets were intensively determined by a series of characterizations. The tribological properties of the as-exfoliated MoS_2 nanosheets were examined by adding oil as an additive. Finally, we discuss the friction reducing and forming mechanisms of the as-exfoliated MoS_2 nanosheets.

2. Experimental section

2.1 Materials and methods

MoS_2 nanosheets were achieved by hydrothermal-shearing exfoliation. Initially, 0.98 g of ammonium carbonate ($(NH_4)_2CO_3$, AC) was dissolved in 20 mL deionized water and then 0.10 g of bulk MoS_2 (Sinopharm Chemical Reagent Co., Ltd) was added into the above solution with magnetic stirring at room temperature for 2 h. Next, the suspension was transferred to a 100 mL Teflon-lined autoclave and heated at 10 rpm and

School of Chemistry and Chemical Engineering, Yangzhou University, Yangzhou 225002, China. E-mail: zlcheng224@126.com

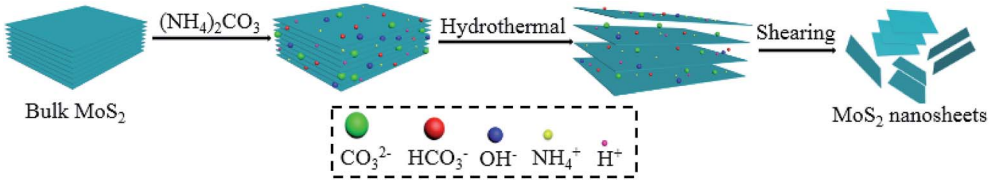

Scheme 1 The forming mechanism of the as-exfoliated MoS_2 nanosheets.

220 °C for 2 h, thus obtaining the sample denoted as MoS_2-AC. Alternatively, the hydrothermal-treated MoS_2 solution was swiftly added into the jug with double four-leaf rotary blades and sheared by the rotary blades at 18 000 rpm for 5 rounds at 2 min on/15 min off. Under severe centrifugal forces, the suspension rapidly diffused from the working area to the stator channel. During the diffusion process, the MoS_2 suspension produced a strong shear force along the tangential direction of the blades (including the lateral shear force, the longitudinal shear force, and the collision). Finally, the upper suspension was washed by deionized water and anhydrous ethanol three times; it was then dried at 60 °C for 24 h and denoted as MoS_2-AC-S. Scheme 1 shows the forming mechanism of as-exfoliated MoS_2 nanosheets. A variety of anions and cations expanded the layer spacing of MoS_2 in the hydrothermal process. During the shearing process, the lateral shear force overcame the weaker van der Waals forces between the MoS_2 layers to obtain less or even a single layer of MoS_2, the longitudinal shear force made MoS_2 nanosheets fracture, and the collision had a synergistic effect.[27]

2.2 Testing of tribological properties

The bulk MoS_2 and as-prepared MoS_2 nanosheets were added in 150 SN base oil using an ultrasonic dispersion, which was marked as MoS_2-based oil, with different concentrations of MoS_2 (0.02 wt%, 0.04 wt%, 0.06 wt%, 0.08 wt% and 0.10 wt%). The tribological performance was detected by a four-ball friction tester (Jinan Chenda Ltd. Co., in China). The testing parameters were set at a speed of 1200 rpm, a stable applied load of 100 N and a duration time of 2 h. Every test was repeated at least three times under the same conditions. At the end of testing, the wear scar diameter was measured using an optical microscope.

2.3 Characterization

XRD patterns, Raman, UV-vis and FTIR spectra were inspected by powder X-ray diffractometer (Bruker AXS, German), inVia Raman spectrometer (Renishaw, Britain), Cary 5000 spectrophotometer (Varian, USA) and Cary 610/670 micro infrared spectrometer (Varian, USA), respectively. The SEM, TEM and HRTEM images were recorded by a S-4800II field-emission scanning electron microscope (Hitachi, Japan), a Tecnai 12 transmission electron microscope (Philips, Netherlands) and a Tecnai G2 F30 S-TWIN field-emission transmission electron microscope (FEI, USA), respectively. The AFM analysis was conducted on a Nanoscope (Digital Instruments, USA). The wear scar micrographs were obtained using a LSM 700 3D laser scanning microscope (CARL ZEISS, Germany).

3. Results and discussion

Fig. 1 shows the XRD patterns and Raman spectra of the bulk MoS_2, MoS_2-AC and MoS_2-AC-S. As shown in Fig. 1a, all the MoS_2 samples show nine peaks at $2\theta = 14.4°$, 32.7°, 33.5°, 35.9°, 39.5°, 44.2°, 49.9°, 58.3° and 60.1°, corresponding to the (002), (100), (101), (102), (103), (006), (105), (110) and (008) planes of 2H MoS_2 (JCPDS no. 37-1492). Every peak is assigned to the lattice of representative MoS_2 and there is no extra peak

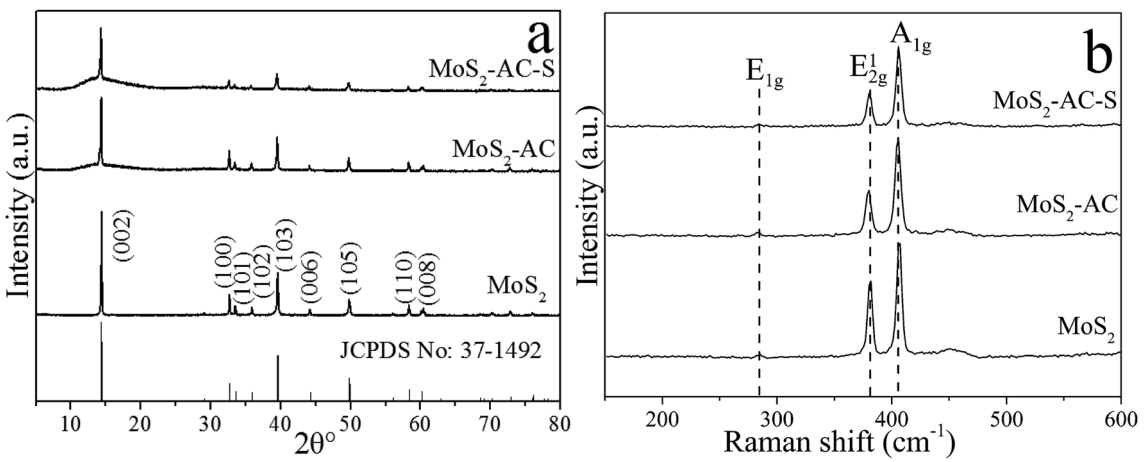

Fig. 1 XRD patterns (a) and Raman spectra (b) of the bulk MoS_2, MoS_2-AC and MoS_2-AC-S.

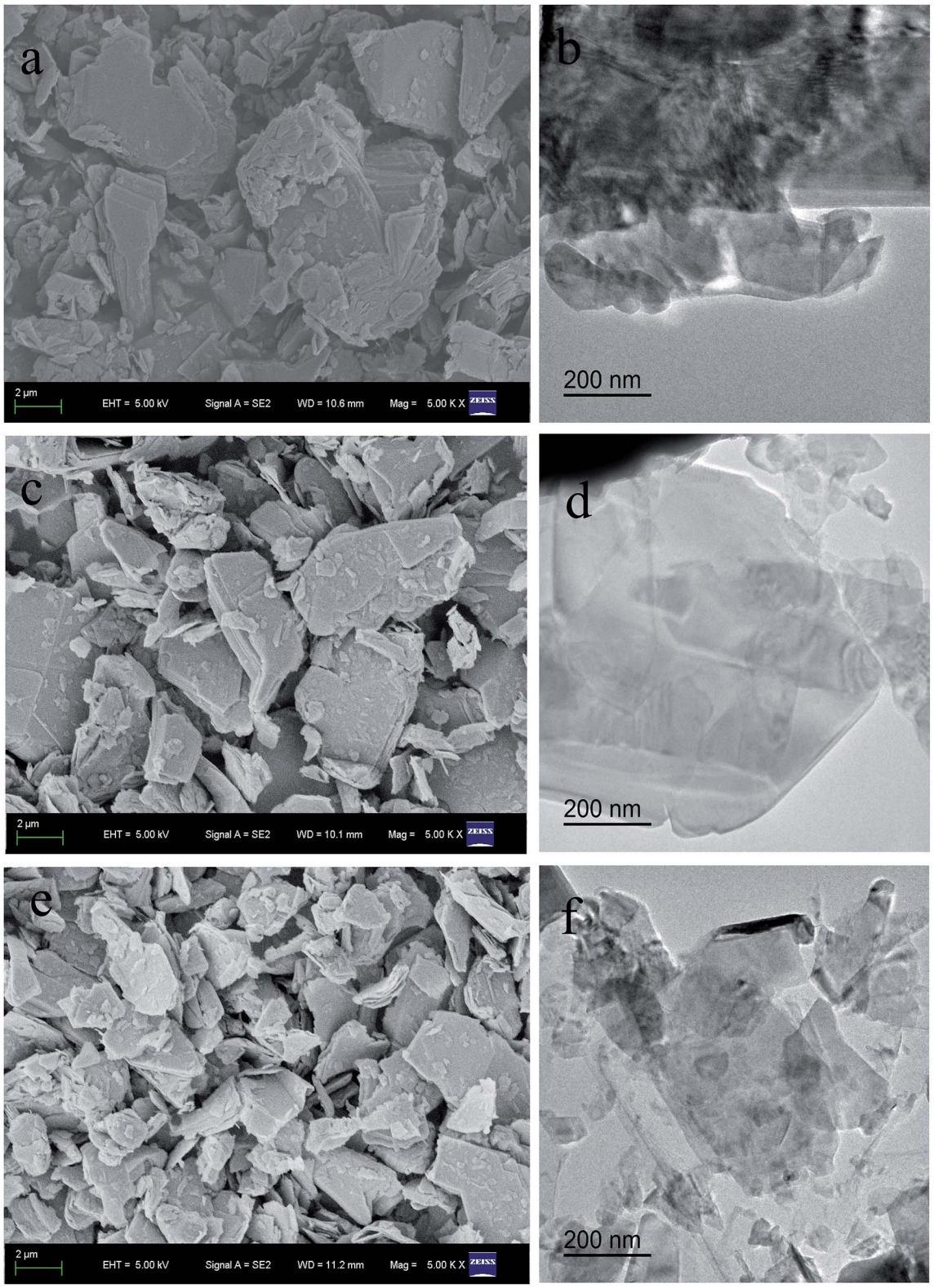

Fig. 2 SEM and TEM images of the bulk MoS_2 (a and b), MoS_2-AC (c and d) and MoS_2-AC-S (e and f).

corresponding to MoO_3. This demonstrates that the as-exfoliated MoS_2 is a single phase.[28] However, all lattice planes of MoS_2-AC and MoS_2-AC-S show weaker peak intensities than the bulk MoS_2. The possible reason is that the MoS_2-AC and MoS_2-AC-S have fewer layers than the bulk MoS_2. In Fig. 1b, the bulk MoS_2, MoS_2-AC and MoS_2-AC-S have two stronger characteristic peaks at about 381 cm^{-1} (E^1_{2g} mode) and 406 cm^{-1} (A_{1g} mode).[29,30] However, the frequency difference between E^1_{2g} and

A_{1g} peaks for the as-exfoliated MoS_2 sample is less than that of the bulk MoS_2. This indicates that the number of as-exfoliated MoS_2 layers decreases after two exfoliation processes.[31,32] In addition, MoS_2-AC-S shows less frequency difference than MoS_2-AC, indicating that the layer of MoS_2-AC-S decreases after shearing. Furthermore, the characteristic peaks of the 1T phase are not observed after the exfoliation process, indicating that there is no phase transition.

As shown in Fig. 2, the bulk MoS_2 had a larger lateral size and thickness (Fig. 2a and b). Evidently, the lateral size and thickness of the MoS_2-AC and MoS_2-AC-S became smaller and thinner (Fig. 2c–f). More importantly, after the hydrothermal process using $(NH_4)_2CO_3$, the exfoliation of bulk MoS_2 into multi-layer occurred. This suggests that $(NH_4)_2CO_3$ in the interlayer of MoS_2 under hydrothermal processing served as the exfoliation agent. In comparison of MoS_2-AC and MoS_2-AC-S, the lateral size and thickness of the latter are further lessened and filmy. The result confirms that the shearing after the hydrothermal process accounts for the deep exfoliation into fewer layers and a smaller size. Accordingly, the combination of the two processes is propitious to the curling of the flake edge and prevents the secondary assembly of nanosheets.[33] The surface area was measured to confirm the changes of the bulk MoS_2 and MoS_2-AC-S nanosheets. The results show that the surface area of MoS_2-AC-S is about 62.86% larger than that of bulk MoS_2, indicating that the exfoliation can increase the surface area (Table 1).

In Fig. 3a and b, the edge layers of the bulk MoS_2 are far more than 20, and the layers of MoS_2-AC are more than 10 and less than the layers of the bulk MoS_2. As displayed in the HRTEM image of Fig. 3c, the thickness of MoS_2-AC-S with 0.62 nm of interlayer basal spacing is up to about 4–6 layers, which corresponds to the (002) plane for MoS_2. Additionally, the 0.27 nm of (100) plane, the 0.23 nm of (103) plane and the 0.16 nm of (110) plane for MoS_2-AC-S is in good agreement with the XRD spectra. The result indicates that the as-exfoliated MoS_2 nanosheets still retain a good crystallinity. Fig. 3d shows the corresponding SAED pattern of MoS_2-AC-S, which reveals the presence of a ring-like pattern, thus corroborating the existence of multi-layer polycrystalline nanosheets.[34] The size and thickness of the as-exfoliated MoS_2-AC-S was further verified by AFM (Fig. 3e). The as-exfoliated MoS_2-AC-S had a larger irregular-shaped size and about 2.70–3.59 nm thickness (calculated layer number about 4–6), which is consistent with the HRTEM result.

Fig. 4 shows the average friction coefficients (COFs) and wear scar diameters (AWSDs) of bulk MoS_2 and as-exfoliated MoS_2 under a rotating speed of 1200 rpm and a load of 100 N. As disclosed in Fig. 4a, the average COFs of the bulk MoS_2-based oil and MoS_2-AC-S-based oil with the increase of adding content are descended prior to 0.06 wt% and 0.08%, respectively. With further increase of adding content, the COFs thereupon rise fleetly. The optimal average COFs of these two samples decreased by about 19.01% and 20.66% compared to that of the 150 SN base oil. This is because MoS_2-AC-S with few layers and small size can more easily enter into the contact surface than the bulk MoS_2, probably forming a tribofilm on the contact surface to reduce the friction coefficient and wear scar diameter.[35] However, excessive MoS_2 can result in a poor dispersion in oil, and the larger agglomerates consisting of nanosheets conversely increase the friction. Moreover, the AWSDs of the bulk MoS_2 and MoS_2-AC-S decrease with the increase in the content up to 0.08 wt%, but the excessive increase in the content could give rise to abrasive wear, for instance at 0.1 wt%. Furthermore, the AWSDs of the base oil containing 0.08 wt% bulk MoS_2 and MoS_2-AC-S are about 40.00% and 47.27% lower than the base oil, respectively.

Fig. 5a and b show the effect of the load on the average COFs and AWSDs of the steel balls lubricated by 0.08 wt% MoS_2-AC-S-based oil with 2 h of friction time. As can be seen from Fig. 5a, the average COFs of MoS_2-AC-S-based oil are decreasing with the increase in the applied load. Furthermore, the COF of MoS_2-AC-S-based oil at 300 N is about 27.18% lower than that of MoS_2-AC-S-based oil at 50 N. This demonstrates that the MoS_2-AC-S-based oil under a higher applied load is more effective to improve the friction ability. On the contrary, the AWSDs of MoS_2-AC-S-based oil increased in the range of testing. The AWSD of MoS_2-AC-S-based oil at 50 N is about 58.33% smaller than that of MoS_2-AC-S-based oil at 300 N. Overall, the MoS_2-AC-S-based oil shows better anti-friction ability at higher applied load and better anti-wear ability at a lower applied load.

Fig. 6 illustrates the COF curves of the base oil, 0.08 wt% bulk MoS_2-based oil and 0.08 wt% MoS_2-AC-S-based oil tested for 2 h. Fig. 6a shows that the COFs of the bulk MoS_2-based oil and MoS_2-AC-S-based oil are lower than that of the 150 SN base oil throughout the testing time. More importantly, the COF and AWSD of the MoS_2-AC-S-based oil are distinctly lower than those of the bulk MoS_2-based oil. Consequently, the average COF and AWSD of MoS_2-AC-S-based oil decreased to about 15.79% and 12.12% compared to those of the bulk MoS_2. The result indicates that the bulk MoS_2 slides difficultly onto the contact surface of the steel ball with the flow of the base oil to reduce the COF and WSD due to the bulk MoS_2 with a large size, greater thickness and poor dispersibility in base oil. Owing to the MoS_2-AC-S with fewer layers and smaller size, it is easy to permeate into the friction surfaces of the counterpart to form a tribofilm.[36] Accidentally, the COF of MoS_2 nanosheets is rising with the friction time. This suggests that the stability of MoS_2 nanosheets in oil is poor in running-in period.

The 3D laser scanning micrograph was used to measure the morphologies of the worn surface for clearly understanding the tribological behavior. Fig. 7 displays the 3D profiles of the worn surfaces of steel balls tested by the base oil, 0.08 wt% bulk MoS_2-based oil and 0.08 wt% MoS_2-AC-S-based oil. The contact areas of the testing balls are all severely damaged to a different degree after 2 h. For the base oil, the worn surface has a very rough wear with a deep and wide hollow along the rubbing direction. However, the worn surfaces of steel balls tested by the bulk MoS_2 and MoS_2-AC-S as additives are much smaller than that of the base oil because of

Table 1 The BET surface area of bulk MoS_2 and MoS_2-AC-S

Samples	Surface area ($m^2\ g^{-1}$)
Bulk MoS_2	15.475
MoS_2-AC-S	25.203

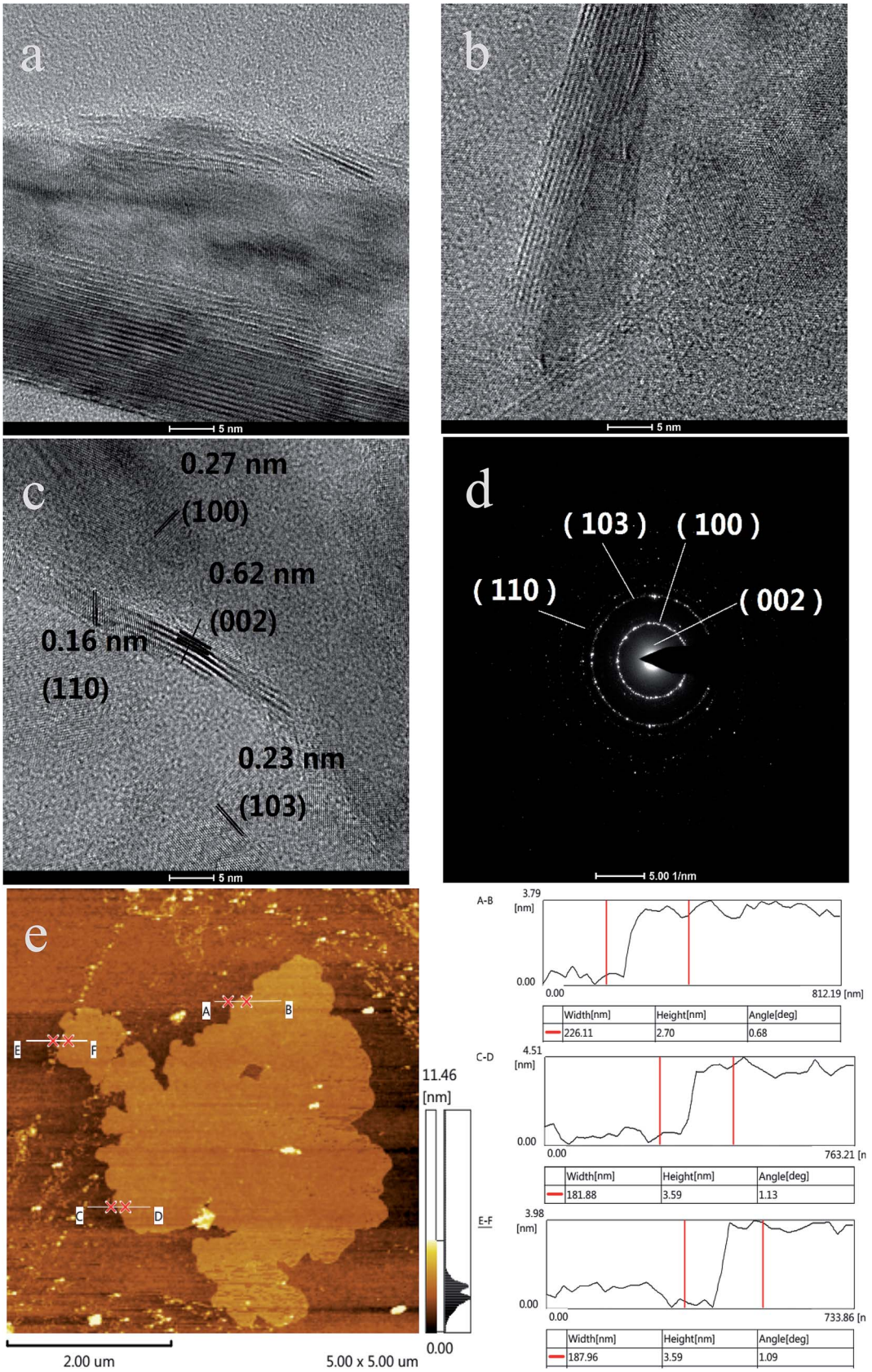

Fig. 3 HRTEM images of bulk MoS_2 (a) and MoS_2-AC (b); HRTEM image (c); SAED pattern; (d) and AFM image and the corresponding height (e) of MoS_2-AC-S.

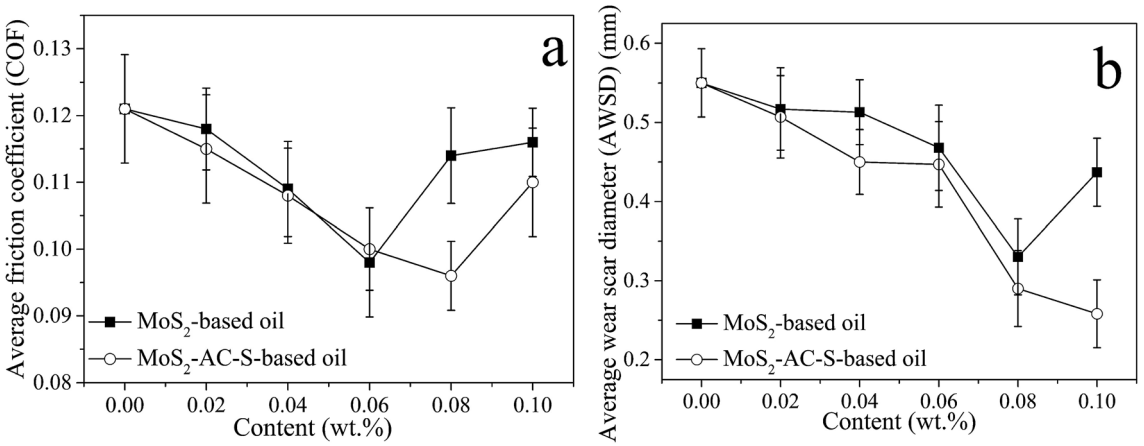

Fig. 4 The average COFs (a) and AWSDs (b) of the bulk MoS_2-based oil and MoS_2-AC-S-based oil as a function of adding content.

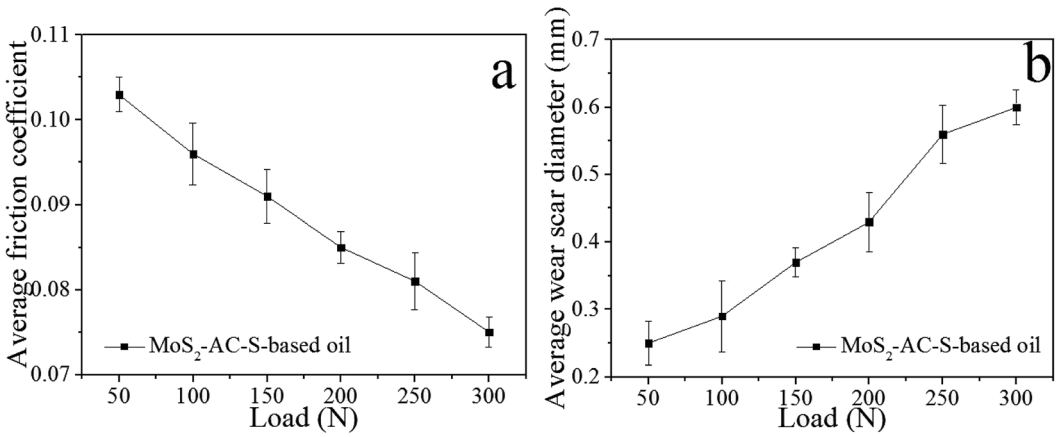

Fig. 5 The average COFs (a) and AWSDs (b) of base oil with 0.08 wt% MoS_2-AC-S as a function of load.

forming the tribofilm on the contact surface, which is derived from the interaction between MoS_2 and friction pairs.[37] For further demonstration of the tribofilm, the worn surfaces of these steel balls were examined by Raman spectroscopy. The spectra corroborate the E^1_{2g} and A_{1g} feature peaks of MoS_2 observed on the worn surfaces tested by the bulk MoS_2-based oil and MoS_2-AC-S-based

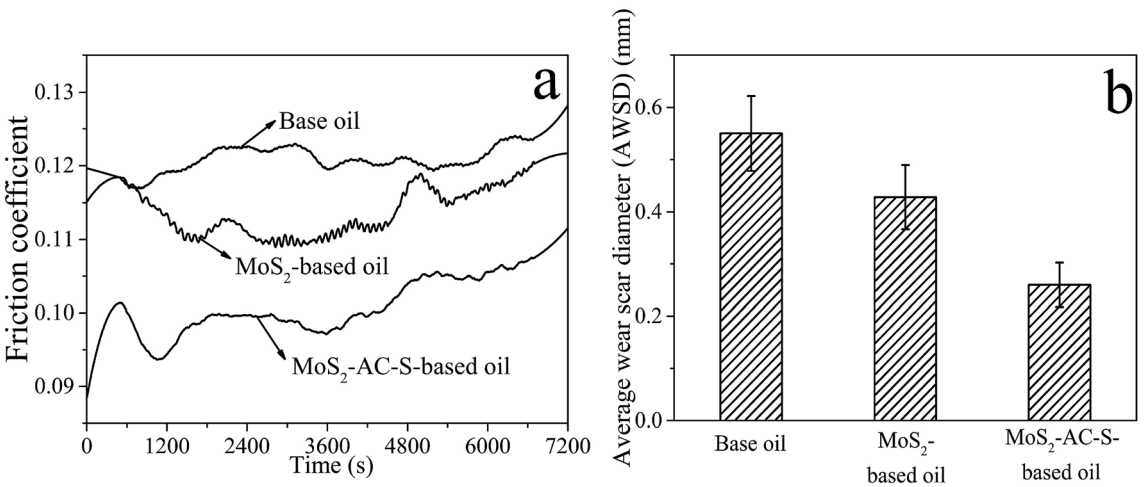

Fig. 6 The COFs (a) and AWSDs (b) of base oil, base oil with 0.08 wt% MoS_2 and base oil with 0.08 wt% MoS_2-AC-S as a function of time.

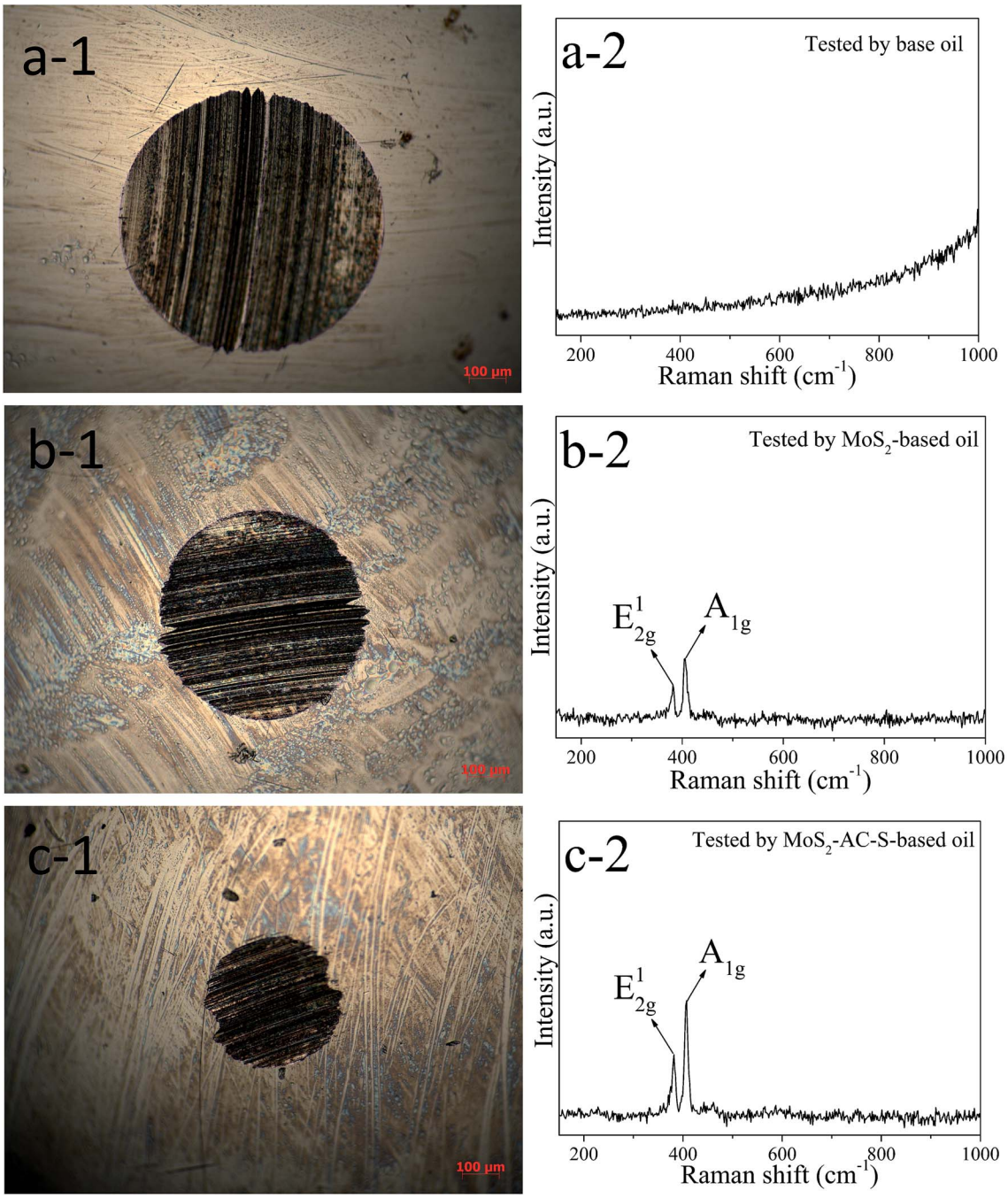

Fig. 7 3D laser scanning micrographs (left) and the corresponding Raman spectra (right) of worn steel ball tested by (a-1 and a-2) base oil, (b-1 and b-2) base oil with 0.08 wt% MoS_2 and (c-1 and c-2) base oil with 0.08 wt% MoS_2-AC-S.

oil. The friction reducing mechanism suggests that the MoS_2 nanosheets in oil can smoothly slide onto the touching surface to avoid the wear of the tested steel ball.[38,39]

4. Conclusions

In summary, 2D MoS_2 nanosheets with 4–6 layers were successfully prepared by the hydrothermal-assisted shearing exfoliation method. During exfoliation processing, the strategy of organic-free was thoroughly achieved. The MoS_2 nanosheets as additives were applied in oil for the sake of anti-friction and anti-wear. The results revealed that the average COF and AWSD of the 150 SN base oil with 0.08 wt% MoS_2 nanosheets decreased to about 20.66% and 47.27% compared to those of the base oil and exhibited better anti-friction and anti-wear performances.

Conflicts of interest

There are no conflicts to declare.

Acknowledgements

This work was funded by Jiangsu Industrial-Academic-Research Prospective Joint Project (BY2016069-02). The authors also acknowledge the Project Funded by the Priority Academic Program Development of Jiangsu Higher Education Institutions. The data of this paper originated from the Test Center of Yangzhou University.

References

1 D. Voiry, M. Salehi, R. Silva, T. Fujita, M. Chen, T. Asefa, V. B. Shenoy, G. Eda and M. Chhowalla, Conducting MoS_2 nanosheets as catalysts for hydrogen evolution reaction, *Nano Lett.*, 2013, **13**(12), 6222–6227.

2 Z. Cui, H. Chu, S. Gao, Y. Pei, J. Jin, Y. Ge, P. Dong, P. M. Ajayan, J. Shen and M. Ye, Large-scale controlled synthesis of porous two-dimensional nanosheets for hydrogen evolution reaction through a chemical pathway, *Nanoscale*, 2018, **10**(13), 6168–6176.

3 G. S. Bang, K. W. Nam, J. Y. Kim, J. Shin, J. W. Choi and S. Y. Choi, Effective liquid-phase exfoliation and sodium ion battery application of MoS_2 nanosheets, *ACS Appl. Mater. Interfaces*, 2014, **6**(10), 7084–7089.

4 B. Guo, F. Yu, X. Chen, B. Li and Y. Ke, Preparation of yolk-shell MoS_2 nanospheres covered with carbon shell for excellent lithium-ion battery anodes, *Appl. Surf. Sci.*, 2017, **434**, 1021–1029.

5 X. Gan, H. Zhao, K.-Y. Wong, D. Y. Lei, Y. Zhang and Q. Xie, Covalent functionalization of MoS_2 nanosheets synthesized by liquid phase exfoliation to construct electrochemical sensors for Cd (II) detection, *Talanta*, 2018, **182**, 38–48.

6 S. Bhattacharjee, K. L. Ganapathi, S. Mohan and N. Bhat, A sub-thermionic MoS_2 FET with tunable transport, *Appl. Phys. Lett.*, 2017, **111**(16), 163501–163505.

7 J. Cao, J. Zhou, Y. Zhang and X. Liu, Theoretical study of H_2 adsorbed on monolayer MoS_2 doped with N, Si, P, *Microelectron. Eng.*, 2018, **190**, 63–67.

8 Y. Gao, K. Huang, X. Wu, Z. Hou and Y. Liu, MoS_2 nanosheets assembling three-dimensional nanospheres for enhanced-performance supercapacitor, *J. Alloys Compd.*, 2018, **741**, 174–181.

9 N. Rajendhran, S. Palanisamy, P. Periyasamy and R. Venkatachalam, Enhancing of the tribological characteristics of the lubricant oils using Ni-promoted MoS_2 nanosheets as nano-additives, *Tribol. Int.*, 2017, **118**, 314–328.

10 P. Wu, Z. Liu and Z. Cheng, Preparation and tribological properties of oleic acid-decorated MoS_2 nanosheets with good oil dispersion, *J. Dispersion Sci. Technol.*, 2018, **39**, 1742–1751.

11 E. Hu, Y. Xu, K. Hu and X. Hu, Tribological properties of 3 types of MoS_2 additives in different base greases, *Lubr. Sci.*, 2017, 1–15.

12 N. Rajendhran, S. Palanisamy, P. Periyasamy and R. Venkatachalam, Enhancing of the tribological characteristics of the lubricant oils using Ni-promoted MoS_2 nanosheets as nano-additives, *Tribol. Int.*, 2017, **118**, 314–328.

13 K. Krishnamoorthy, P. Pazhamalai, G. Kumar Veerasubramani and S. J. Kim, Mechanically delaminated few layered MoS_2 nanosheets based high performance wire type solid-state symmetric supercapacitors, *J. Power Sources*, 2016, **321**, 112–119.

14 X. You, N. Liu, C. J. Lee and J. P. James, An electrochemical route to MoS_2 nanosheets for device applications, *Mater. Lett.*, 2014, **121**(2), 31–35.

15 S. Ji, Z. Yang, C. Zhang, Z. Liu, W. W. Tjiu, I. Y. Phang, Z. Zhang, J. Pan and T. Liu, Exfoliated MoS_2 nanosheets as efficient catalysts for electrochemical hydrogen evolution, *Electrochim. Acta*, 2013, **109**(11), 269–275.

16 G. S. Bang, K. W. Nam, J. Y. Kim, J. Shin, J. W. Choi and S.-Yool Choi, Effective liquid-phase exfoliation and sodium ion battery application of MoS_2 nanosheets, *ACS Appl. Mater. Interfaces*, 2014, **6**(10), 7084–7089.

17 E. Varrla, C. Backes, K. R. Paton, A. Harvey, Z. Gholamvand, J. McCauley and J. N. Coleman, Large-scale production of size-controlled MoS_2 nanosheets by shear exfoliation, *Chem. Mater.*, 2015, **27**, 1129–1139.

18 X. Wang, H. Feng, Y. Wu and L. Jiao, Controlled synthesis of highly crystalline MoS_2 flakes by chemical vapor deposition, *J. Am. Chem. Soc.*, 2013, **135**(14), 5304–5307.

19 S. Kumari, R. Gusain, N. Kumar and O. P. Khatri, PEG-mediated hydrothermal synthesis of hierarchical microspheres of MoS_2 nanosheets and their potential for lubrication application, *J. Ind. Eng. Chem.*, 2016, **42**, 87–94.

20 H. Huang, X. Feng, C. Du and W. Song, High-quality phosphorus-doped MoS_2 ultrathin nanosheets with amenable ORR catalytic activity, *Chem. Commun.*, 2015, **51**(37), 7903–7906.

21 G. S. Bang, K. W. Nam, J. Y. Kim, J. Shin, J. W. Choi and S.-Y. Choi, Effective liquid-phase exfoliation and sodium ion battery application of MoS_2 nanosheets, *ACS Appl. Mater. Interfaces*, 2014, **6**(10), 7084–7089.

22 S. Ji, Z. Yang, C. Zhang, Z. Liu, W. W. Tjiu, In Y. Phang, Z. Zhang, J. Pan and T. Liu, Exfoliated MoS_2 nanosheets as efficient catalysts for electrochemical hydrogen evolution, *Electrochim. Acta*, 2013, **109**(11), 269–275.

23 E. Varrla, C. Backes, K. R. Paton, A. Harvey, Z. Gholamvand, J. McCauley and J. N. Coleman, Large-scale production of size-controlled MoS_2 nanosheets by shear exfoliation, *Chem. Mater.*, 2015, **27**, 1129–1139.

24 E. Varrla, C. Backes, K. R. Paton, A. Harvey, Z. Gholamvand, J. McCauley and J. N. Coleman, Large-scale production of size-controlled MoS_2 nanosheets by shear exfoliation, *Chem. Mater.*, 2015, **27**, 1129–1139.

25 Y. Li, X. Yin and W. Wu, Preparation of few-layer MoS_2 nanosheets *via* an efficient shearing exfoliation method, *Ind. Eng. Chem. Res.*, 2018, **57**, 2838–2846.

26 H. Yu, H. Zhu, M. Dargusch and Y. Huang, A reliable and highly efficient exfoliation method for water-dispersible MoS_2 nanosheet, *J. Colloid Interface Sci.*, 2018, **514**, 642–647.

27 Y. Li, X. Yin and W. Wu, Preparation of few-layer MoS_2 nanosheets *via* an efficient shearing exfoliation method, *Ind. Eng. Chem. Res.*, 2018, **57**, 2838–2846.

28 Y. Zhang, L. Zuo, Y. Huang, L. Zhang, F. Lai, W. Fan and T. Liu, In-situ growth of few-layered MoS_2 nanosheets on highly porous carbon aerogel as advanced electrocatalysts for hydrogen evolution reaction, *ACS Sustainable Chem. Eng.*, 2015, **3**(12), 3140–3148.

29 D. Wang, X. Zhang, S. Bao, Z. Zhang, H. Fei and Z. Wu, Phase-engineering of multiphasic 1T/2H MoS_2 catalyst for highly efficient hydrogen evolution, *J. Mater. Chem. A*, 2017, **5**, 2681–2688.

30 P. Wu, Y. Feng, T. Ge, Y. Kong, Z. Ma, Z. Liu and Z. Cheng, An investigation on tribological properties of the chemically capped zinc borate (ZB)/MoS_2 nanocomposites in oil, *J. Ind. Eng. Chem.*, 2018, **63**, 157–167.

31 S. Wu, H. Huang, M. Shang, C. Du, Y. Wu and W. Song, High visible light sensitive MoS_2 ultrathin nanosheets for photoelectrochemical biosensing, *Biosens. Bioelectron.*, 2016, **92**, 646–653.

32 M. Li, D. Wang, J. Li, Z. Pan, H. Ma, Y. Jiang and Z. Tian, Facile hydrothermal synthesis of MoS_2 nano-sheets with controllable structures and enhanced catalytic performance for anthracene hydrogenation, *RSC Adv.*, 2016, **6**(75), 71534–71542.

33 L. Chen, T. Wang, Y. Wu, F. Ma, G. Zhao and X. Hao, Fabrication of two-dimensional nanosheets *via* water freezing expansion exfoliation, *Nanotechnology*, 2014, **25**, 495302.

34 J. Wu, J. Dai, Y. Shao, M. Cao and X. Wu, Carbon dot-assisted hydrothermal synthesis of flower-like MoS_2 nanospheres constructed by few-layered multiphase MoS_2 nanosheets for supercapacitors, *RSC Adv.*, 2016, **6**, 77999–78007.

35 P. Wu, Z. Cheng, Y. Kong, Z. Ma and Z. Liu, Templated synthesis of plate-like MoS_2 nanosheets assisted with HNTs and their tribological performance in oil, *J. Nanopart. Res.*, 2018, **20**, 138.

36 P. Wu, Z. Cheng, Y. Kong, Z. Ma and Z. Liu, Templated synthesis of plate-like MoS_2 nanosheets assisted with HNTs and their tribological performance in oil, *J. Nanopart. Res.*, 2018, **20**, 138.

37 C. Yang, X. Hou, Z. Li, X. Li, L. Yu and Z. Zhang, Preparation of surface-modified lanthanum fluoride-graphene oxide nanohybrids and evaluation of their tribological properties as lubricant additive in liquid paraffin, *Appl. Surf. Sci.*, 2016, **388**, 497–502.

38 L. Zhang, H. Yi, S. Feng, L. Zhang, L. Zhang, Z. Jiao, Y. Zhan and Y. Wang, Preparation and tribological properties of novel boehmite/graphene oxide nano-hybrid, *Ceram. Int.*, 2016, **42**, 6178–6186.

39 P. Wu, Z. Liu and Z. Cheng, Growth of MoS_2 nanotubes templated by halloysite nanotubes for the reduction of friction in oil, *ACS Omega*, 2018, **3**, 15002–15008.